Nitric oxide–dependent Src activation and resultant caveolin-1 phosphorylation promote eNOS/caveolin-1 binding and eNOS inhibition

Zhenlong Chen[a], Farnaz R. Bakhshi[a], Ayesha N. Shajahan[b], Tiffany Sharma[a], Mao Mao[c], Andy Trane[d], Pascal Bernatchez[d], Geerten P. van Nieuw Amerongen[e], Marcelo G. Bonini[a,c], Randal A. Skidgel[a,f], Asrar B. Malik[a,f], and Richard D. Minshall[a,f,g]

[a]Department of Pharmacology, University of Illinois, Chicago, IL 60612; [b]Lombardi Comprehensive Cancer Center, Georgetown University, Washington, DC 20057; [c]Department of Medicine, University of Illinois, Chicago, IL 60612; [d]Department of Anesthesiology, Pharmacology and Therapeutics, University of British Columbia, James Hogg Research Centre, Providence Heart and Lung Institute, St. Paul's Hospital, Vancouver, BC V6Z 1Y6, Canada; [e]Department for Physiology, Institute for Cardiovascular Research, VU University Medical Center, 1081 BT Amsterdam, Netherlands; [f]Center for Lung and Vascular Biology and [g]Department of Anesthesiology, University of Illinois, Chicago, IL 60612

ABSTRACT **Endothelial nitric oxide synthase (eNOS)–mediated NO production plays a critical role in the regulation of vascular function and pathophysiology. Caveolin-1 (Cav-1) binding to eNOS holds eNOS in an inactive conformation; however, the mechanism of Cav-1–mediated inhibition of activated eNOS is unclear. Here the role of Src-dependent Cav-1 phosphorylation in eNOS negative feedback regulation is investigated. Using fluorescence resonance energy transfer (FRET) and coimmunoprecipitation analyses, we observed increased interaction between eNOS and Cav-1 following stimulation of endothelial cells with thrombin, vascular endothelial growth factor, and Ca^{2+} ionophore A23187, which is corroborated in isolated perfused mouse lung. The eNOS/Cav-1 interaction is blocked by eNOS inhibitor L-N^G-nitroarginine methyl ester (hydrochloride) and Src kinase inhibitor 4-amino-5-(4-chlorophenyl)-7-(*t*-butyl) pyrazolo [3, 4-*d*] pyrimidine. We also observe increased binding of phosphomimicking Y14D-Cav-1 mutant transduced in human embryonic kidney cells overexpressing eNOS and reduced Ca^{2+}-induced NO production compared to cells expressing the phosphodefective Y14F-Cav-1 mutant. Finally, Src FRET biosensor, eNOS small interfering RNA, and NO donor studies demonstrate NO-induced Src activation and Cav-1 phosphorylation at Tyr-14, resulting in increased eNOS/Cav-1 interaction and inhibition of eNOS activity. Taken together, these data suggest that activation of eNOS promotes Src-dependent Cav-1–Tyr-14 phosphorylation and eNOS/Cav-1 binding, that is, eNOS feedback inhibition.**

Monitoring Editor
Robert G. Parton
University of Queensland

Received: Sep 26, 2011
Revised: Jan 18, 2012
Accepted: Feb 3, 2012

This article was published online ahead of print in MBoC in Press (http://www.molbiolcell.org/cgi/doi/10.1091/mbc.E11-09-0811) on February 9, 2012.

Address correspondence to: Richard D. Minshall (rminsh@uic.edu).

Abbreviations used: A23187, calcium ionophore; CaM, calmodulin; Cav-1, caveolin-1; CFP, cyan fluorescent protein; coIP, coimmunoprecipitation; eNOS, endothelial nitric oxide synthase; FRET, fluorescence resonance energy transfer; HEK, human embryonic kidney; HUVEC, human umbilical vascular endothelial cell; L-NAME, L-N^G-nitroarginine methyl ester (hydrochloride); NO, nitric oxide; PP2, 4-amino-5-(4-chlorophenyl)-7-(*t*-butyl) pyrazolo [3, 4-*d*] pyrimidine; Src, Src-family kinase; VEGF, vascular endothelial growth factor; YFP, yellow fluorescent protein.

INTRODUCTION

Production of nitric oxide (NO) by endothelial cell nitric oxide synthase (eNOS; NOS3) regulates vascular tone, blood flow, leukocyte-endothelial interactions, platelet adhesion and aggregation, and vascular smooth muscle cell proliferation (Sessa, 2004; Atochin and Huang, 2010). Studies demonstrated direct interaction of eNOS with caveolin-1 (Cav-1; Feron *et al*., 1996; García-Cardeña *et al*., 1996) and that Cav-1 functions as an endogenous negative regulator of eNOS activity (Drab *et al*., 2001; Razani *et al*., 2001; Zhao *et al*., 2002; Wunderlich *et al*., 2006; Maniatis *et al*., 2008). Specifically, eNOS binds to the caveolin scaffold domain (CSD; amino acids 82–101; García-Cardeña *et al*., 1997; Bucci *et al*., 2000), and alanine scanning of the CSD identified Thr-90 and -91 and Phe-92 as

Supplemental Material can be found at:
http://www.molbiolcell.org/content/suppl/2012/02/06/mbc.E11-09-0811.DC1.html

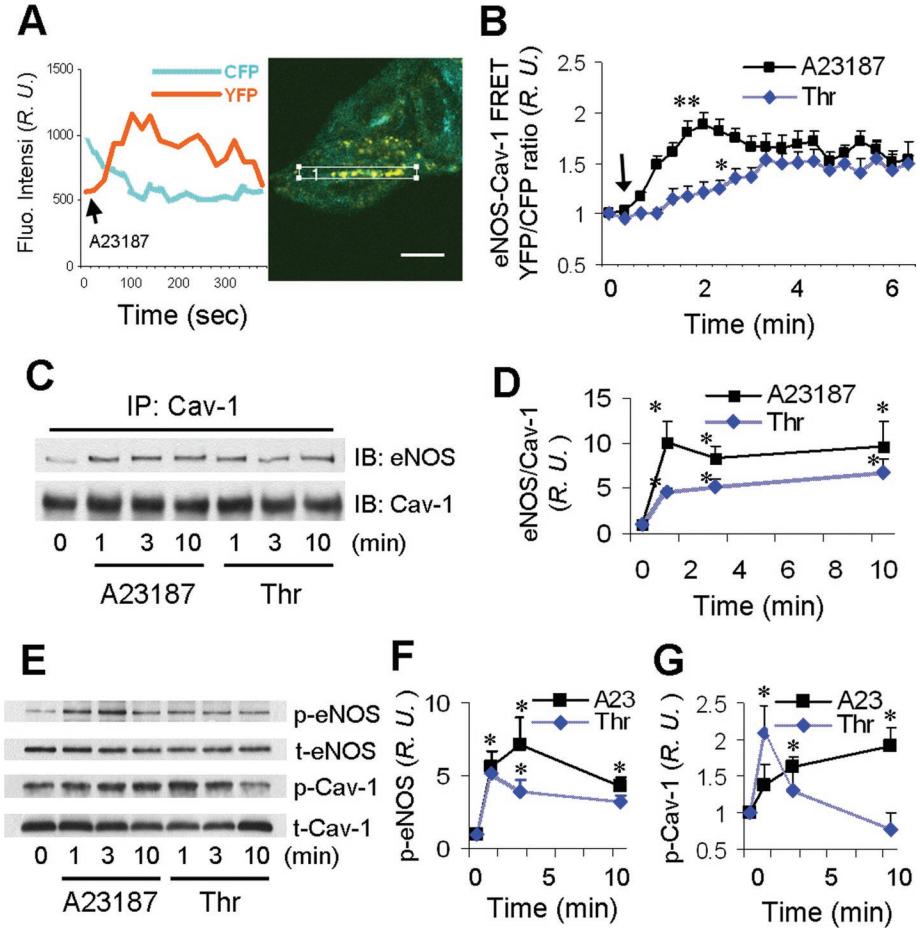

FIGURE 1: Interaction of Cav-1 and eNOS determined by FRET and coIP. (A) Typical FRET image of Cav-1–YFP and eNOS–CFP expressed in CHO cells. Note that the fluorescence intensity of YFP increases, whereas CFP decreases in the ROI (white box) after addition of 5 μM Ca^{2+} ionophore A23187. Bar, 10 μm. (B) Normalized FRET measurements in CHO cells expressing Cav-1–YFP and eNOS–CFP after treatment with 5 μM A23187 (mean ± SEM; n = 12) or 4 U/ml thrombin (mean ± SEM; n = 5). YFP/CFP was normalized as 1 by the value at time zero (*p < 0.01 for all times beyond 2 min after thrombin addition; **p < 0.005 for all times beyond 1.5 min after A23187). (C) CoIP between Cav-1–YFP and eNOS–CFP in CHO cells (mean ± SEM; n = 3). (D) Normalized data of coIP (ratio of eNOS-CFP/Cav-1-YFP after IP with anti–Cav-1 antibody; *p < 0.05). (E) Phosphorylation of Cav-1–YFP and eNOS–CFP in CHO cells after treatment with 5 μM A23187 or 4 U/ml thrombin (mean ± SEM; n = 3). Ratio of phosphorylated/total protein at 0 min was set as 1 (*p < 0.05).

being critical for eNOS binding and inhibition (Bernatchez *et al.*, 2005, 2011). On stimulus-dependent activation of endothelial cells, Cav-1–mediated negative regulation of eNOS can be overcome by Ca^{2+}-calmodulin (CaM), thus increasing eNOS activity (Michel *et al.*, 1997a, 1997b). In contrast, eNOS translocation to internal membranes and CaM dissociation were proposed to participate in the mechanism of eNOS inhibition (Dudzinski and Michel, 2007).

Dudzinski and Michel (2007) proposed that eNOS is negatively regulated by posttranslational lipid modification. Quiescent eNOS is anchored to the caveolar membrane by myristoylation, and thus upon stimulus-dependent activation, Cav-1 binding may be displaced by Ca^{2+}-CaM, enabling eNOS activation. eNOS is then believed to translocate from caveolae to internal membranes, where CaM dissociates, allowing for eNOS reassociation with Cav-1. Müller-Esterl's lab and also Barrett and coworkers proposed that following activation, eNOS translocation back to caveolae results in eNOS inactivation (Oess *et al.*, 2006; Wang *et al.*, 2009). Both of these mechanisms predict that eNOS binding to Cav-1 leads to inhibition of eNOS activity. However, the molecular mechanisms responsible for restoring eNOS enzymatic activity to its basal state and whether its binding to Cav-1 is important in this process have not been established. In the present study, we tested the hypothesis that in endothelial cells, there is an intrinsic NO-dependent mechanism of eNOS negative feedback regulation dependent on phospho–Cav-1 binding.

RESULTS

Kinetics of interaction between eNOS and Cav-1

To assess spatial and temporal eNOS and Cav-1 binding, CHO cells were transfected with fluorescent protein conjugates, and stimulation-dependent fluorescence resonance energy transfer (FRET) was determined. A typical FRET image observed upon stimulation with 5 μM Ca^{2+} ionophore A23187 is shown in Figure 1A. Fluorescence intensity of eNOS–cyan fluorescent protein (CFP; donor) decreased, whereas Cav-1–yellow fluorescent protein (YFP; acceptor) increased in the region of interest (ROI; white box), indicating increased FRET from eNOS to Cav-1 was induced by increased intracellular Ca^{2+} (Figure 1A). After the cells were treated with 5 μM A23187, we observed Cav-1–eNOS FRET that peaked 1.5 min after stimulation and remained elevated for 5 min (Figure 1B). Following thrombin (4 U/ml) treatment, Cav-1–eNOS FRET was also increased at 5 min (Figure 1B). Immunoprecipitation experiments showed that Cav-1–YFP binding to eNOS-CFP increased 10-fold 1 min after addition of A23187 and 5-fold 1 min after stimulation with thrombin compared with medium alone (Figure 1, C and D). To ensure that the expressed fluorescent Cav-1 and eNOS proteins were functional, CHO cells stably expressing Cav-1–YFP and eNOS–CFP were stimulated with A23187 or thrombin, and Western blotting was used to assess the phosphorylation state of Cav-1 and eNOS (Figure 1, E–G). Thus Cav-1 and eNOS phosphorylation increased in parallel with the increase in coimmunoprecipitation (coIP).

Cav-1/eNOS interaction in mouse lung treated with A23187

To assess the in vivo reality of the foregoing observations, we investigated eNOS and Cav-1 interaction in intact vessels of isolated mouse lungs perfused with 5 μM A23187 via pulmonary artery cannula. The whole-lung homogenates were prepared and immunoprecipitated with anti–Cav-1 antibody and probed for both Cav-1 and eNOS (Figure 2A). eNOS binding to Cav-1 increased sixfold after 3 min of treatment with A23187 (Figure 2B). Phosphorylation of eNOS (Ser-1177) increased about fourfold at 3 min following treatment with 5 μM A23187 and then declined compared with medium alone. However, phosphorylation of Src (Tyr-418) and Cav-1 (Tyr-14) continued to increase through 10 min after addition of 5 μM A23187 in mouse lungs (Figure 2, C and D).

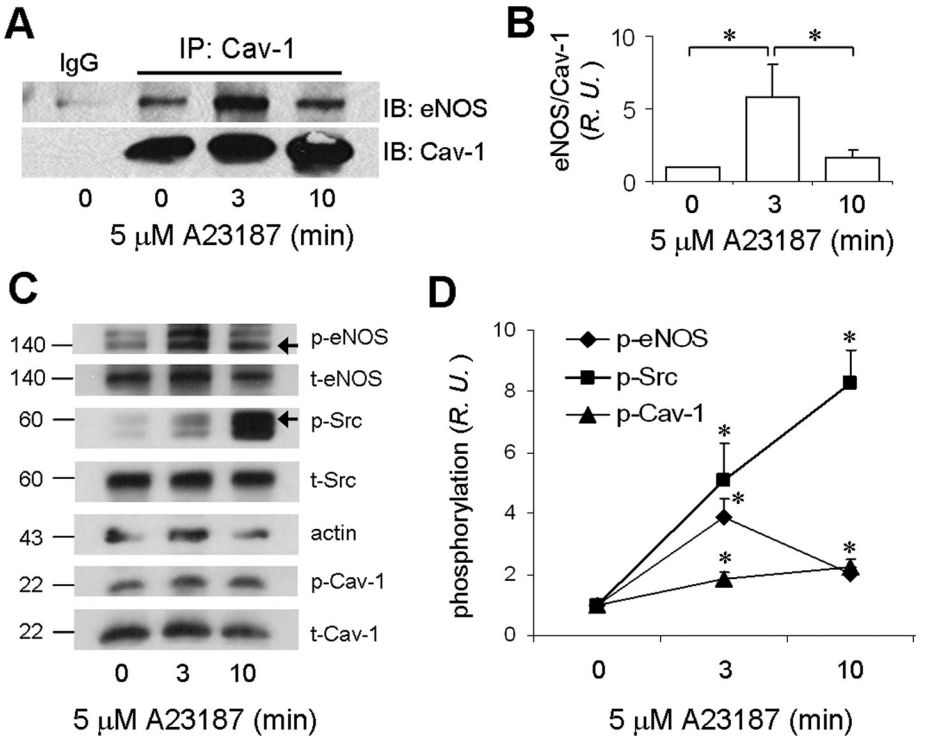

FIGURE 2: CoIP between eNOS and Cav-1 in mouse lung. (A) Mouse lungs were perfused with medium containing 5 μM A23187 for 0, 3, and 10 min. Lungs were then homogenized and prepared for IP with polyclonal anti–Cav-1. (B) Normalized coIP data (mean ± SEM; n = 4); ratio of eNOS/Cav-1 at 0 min was set as 1 (*p < 0.05). (C) Phosphorylation of eNOS–Ser-1177, Src–Tyr-418, and Cav-1–Tyr-14 (indicated by arrows) in mouse lung homogenates following A23187 treatment (D). Normalized ratio of phosphorylated/total protein, with time 0 set as 1 (*p < 0.05; mean ± SEM; n = 4).

Cav-1 and eNOS phosphorylation induces Cav-1/eNOS interaction

Stimulation of human umbilical vascular endothelial cells (HUVECs) with 5 μM A23187, 4 U/ml thrombin, or 20 ng/ml vascular endothelial growth factor (VEGF) increased eNOS activity, as measured by 4,5-diaminofluorescein-2 diacetate (DAF-2 DA) fluorescence intensity, by 7.2-, 6.5-, and 4.6-fold, respectively, over untreated HUVECs (Supplemental Figure S1A). NO release was maximal 1 min after addition of 5 μM A23187, returning toward prestimulation levels by 3 min, and was near basal thereafter (Supplemental Figure S1B). eNOS–Ser-1177 phosphorylation also increased upon stimulation, reaching maximal levels after 3 min (thrombin, 6.0-fold increase; A23187, 5.0-fold; VEGF, 3.9-fold), and then decreased over the next 30 min (Figure 3A). Cav-1–Tyr-14 phosphorylation also increased but at a slower rate than that of eNOS (Figure 3A). The interaction between eNOS and Cav-1 after stimulation of HUVECs was also assessed by coIP (Figure 3B). Enhanced eNOS–Cav-1 association was observed within 1 min of stimulation with A23187, peaked at 5 min (a 5-fold increase compared with untreated cells), and remained elevated at 2.5-fold above baseline at 30 min (Figure 3B).

For Western blots and IP experiments, we isolated total membrane fractions (Supplemental Figure S2) as described in *Materials and Methods*, which contained virtually all of the eNOS and Cav-1 protein relative to membrane-enriched fractions used in previous studies (Busconi and Michel, 1993; Feron *et al.*, 1998). As expected, we also observed increased CaM coIP with eNOS following addition of A23187 (Supplemental Figure S3).

Because both eNOS and Cav-1 phosphorylation increased upon stimulation with A23187, we addressed whether eNOS/Cav-1 interaction required eNOS and Cav-1 phosphorylation. HUVECs were lysed and prepared for IP by anti–p-Ser-1177-eNOS antibody (Figure 3C) under the same conditions as described earlier (Figure 3, A and B). p-Ser-1177-eNOS phosphorylation increased following ionophore stimulation, and the amount of p-Tyr-14-Cav-1 (relative to the amount of total Cav-1) that coimmunoprecipitated with p-Ser-1177-eNOS also increased fivefold relative to vehicle-treated control cells (Figure 3D).

We next determined the effect of eNOS inhibitor L-N^G-nitroarginine methyl ester (hydrochloride) (L-NAME) and Src kinase inhibitor 4-amino-5-(4-chlorophenyl)-7-(*t*-butyl) pyrazolo [3, 4-*d*] pyrimidine (PP2) on the A23187-induced eNOS/Cav-1 interaction. Confluent HUVEC cultures were pretreated with medium alone, 1 mM L-NAME, or 15 μM PP2 for 30 min at 37°C, and then 5 μM A23187 was added to cells and incubated for another 5 min. eNOS, Src, and Cav-1 phosphorylation increased significantly to 4.4-, 1.3-, and 2.6-fold of vehicle-treated cells (1.0 relative unit [R.U.]), respectively (Figure 3E). Pretreatment with L-NAME significantly decreased ionophore-induced increase in Src p-Tyr-418 by 51% (from 0.337 ± 0.067 to 0.164 ± 0.094 R.U. above vehicle-treated cells; p < 0.05; n = 9) and p-Tyr-14-Cav-1 by 68%, whereas PP2 prevented A23187-induced phosphorylation of Src and Cav-1. eNOS–Ser-1177 phosphorylation induced by A23187 was not significantly affected by either PP2 or L-NAME. CoIP experiments showed that eNOS binding to Cav-1 increased eightfold after 5 min treatment with 5 μM A23187 compared with medium alone, and, of interest, both L-NAME and PP2 significantly reduced the interaction between eNOS and Cav-1 (Figure 3F). Thus, PP2 inhibition of Src activity and Cav-1 phosphorylation, as well as L-NAME inhibition of eNOS activity, significantly blocked Ca^{2+}-induced eNOS/Cav-1 binding in endothelial cells.

In additional studies, we assessed the role of various kinases, including Akt, PKA, AMPK, and CaMKII, in the mechanism of eNOS phosphorylation/activation in HUVECs stimulated with Ca^{2+} ionophore A23187 (Supplemental Figure S4). On stimulation, p-eNOS (Ser-1177) and p-Cav-1 (Tyr-14) peaked within 3–5 min, whereas pAkt–Thr-308 was maximal at 20 min and Akt–pSer-473 was maximal at 60 min (Supplemental Figure S4, A–E). Thus eNOS activation occurred at a faster rate than Akt activation, leading us to conclude that Akt does not play a significant role in the early phase of Ca^{2+}-induced eNOS activation. Furthermore, we assessed eNOS–Ser-1177 phosphorylation induced by A23187 following 30 min of pretreatment of cells with 10 μM H89 (PKA inhibitor), 30 μM 5-iodotubercidin (AMPK inhibitor), or 10 μM STO-609 (CaMKII inhibitor). We observed that only the CaMKII inhibitor STO-609 significantly blocked Ca^{2+}-induced eNOS–Ser-1177 phosphorylation by 50% (Supplemental Figure S4, F and G).

p-Tyr-14-Cav-1 promotes eNOS binding and decreases eNOS activity

To further clarify the role of Cav-1 versus eNOS phosphorylation in enhanced binding of eNOS to Cav-1, we coexpressed either

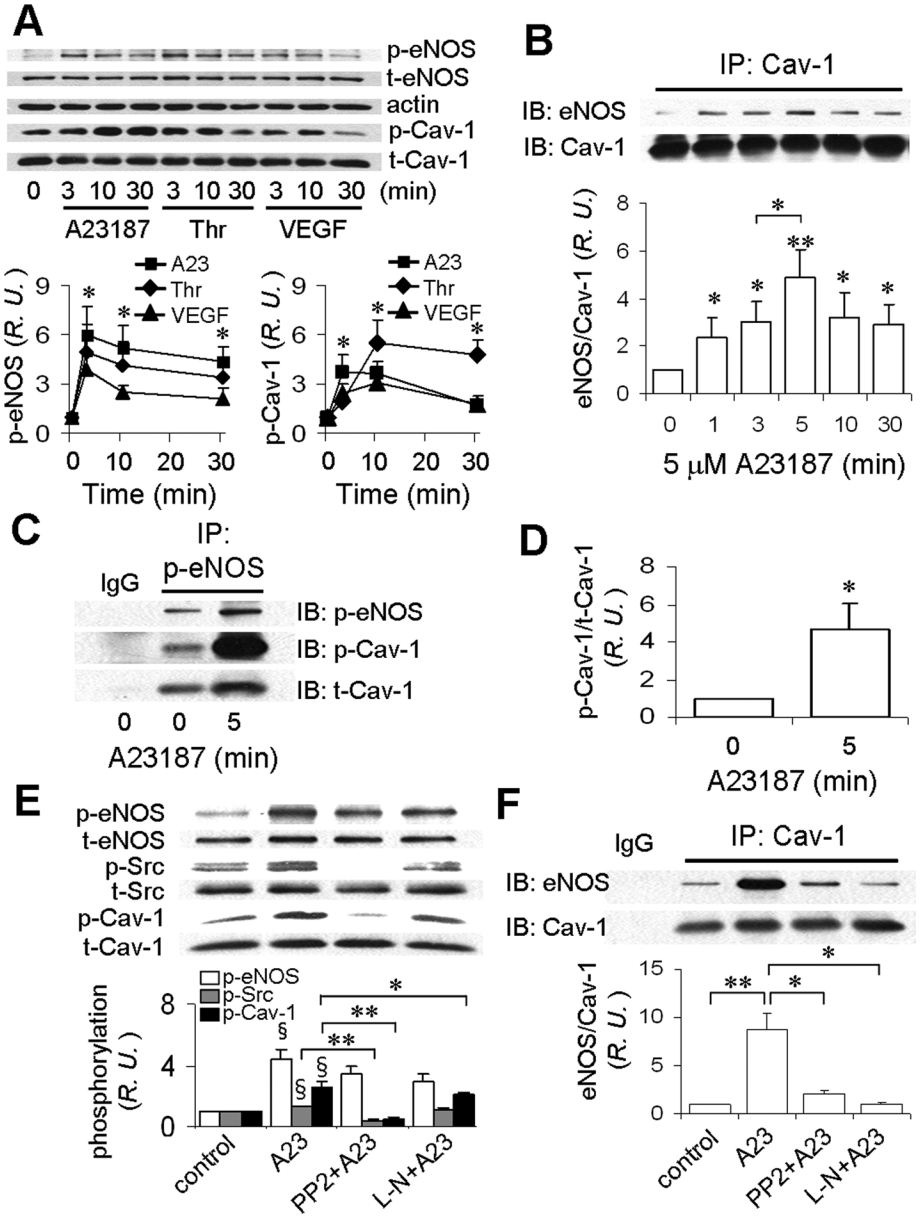

FIGURE 3: Phosphorylation-dependent interaction of eNOS and Cav-1 in HUVEC. (A) Time course of phosphorylation of eNOS–Ser-1177 and Cav-1–Tyr-14 in HUVECs after addition of 5 μM A23187, 4 U/ml thrombin, or 20 ng/ml VEGF (mean ± SEM; n = 6). Normalized data are shown in the bottom two rows (*$p < 0.05$). (B) CoIP of eNOS and Cav-1 in HUVEC after stimulation with 5 μM A23187 at indicated times (mean ± SEM; n = 4. *$p < 0.05$; **$p < 0.005$). (C, D) CoIP of phosphorylated eNOS and Cav-1 in HUVECs treated with A23187 for 5 min at 37°C (mean ± SEM; n = 3). p-Ser-1177-eNOS antibody was used for IP. Normalized data (p-Tyr-14-Cav-1 vs. t-Cav-1 bound to p-eNOS) is shown in D (*$p < 0.05$). (E) Effects of L-NAME and PP2 on phosphorylation of eNOS–Ser-1177, Src–Tyr-418, and Cav-1–Tyr-14 in HUVECs (mean ± SEM; n = 9). Confluent HUVECs were pretreated with 1 mM L-NAME or 15 μM PP2 for 30 min at 37°C prior to addition of 5 μM A23187 (§$p < 0.001$; *$p < 0.05$; and **$p < 0.001$). (F) Effect of L-NAME and PP2 on coIP between eNOS and Cav-1 (mean ± SEM; n = 6) in HUVEC (*$p < 0.05$; **$p < 0.005$).

wild-type (WT) Cav-1, phosphomimicking Y14D-Cav-1 mutant, or phosphodefective Y14F-Cav-1 mutant in human embryonic kidney (HEK) cells together with WT, phosphomimicking (S1177D), or phosphodefective (S1177A) eNOS constructs. We then assessed whether expression of Y14D-Cav-1 promoted the binding of WT-eNOS as compared with phosphodefective eNOS (S1177A) in the absence of stimulation. We also measured eNOS activity in each instance. These experiments involved the transient transfection of WT-eNOS-CFP, eNOS-S1177D-CFP, and eNOS-S1177A-CFP in HEK cells stably expressing WT-Cav-1-YFP, Y14D-Cav-1-YFP, or Y14F-Cav-1-YFP. Cells were lysed 48 h after transfection and immunoprecipitated with anti–Cav-1 antibody. Both eNOS and Cav-1 were measured by Western blot after IP (Figure 4A), and the data from three separate experiments were averaged as shown in the bar graph. We observed Y14D-Cav-1 binding to either WT-eNOS or S1177D-eNOS to be equivalent but 4.2-fold greater than the binding of WT-eNOS and WT-Cav-1, indicating that Cav-1 phosphorylation is an important determinant of eNOS binding. Moreover, binding of the phosphodefective S1177A-eNOS mutant to WT- or Y14D-Cav-1 was significantly reduced, suggesting eNOS phosphorylation is also an important determinant of the binding reaction. Y14F-Cav-1 showed much lower binding to all eNOS constructs compared with WT- or Y14D-Cav-1, suggesting the phospho-defective Cav-1 conformation does not bind well to eNOS (Figure 4A). The level of protein expression achieved with each Cav-1 and eNOS construct before IP was similar, as shown in Figure 4B, and coIP of untagged proteins yielded similar results.

We next determined whether enhanced eNOS binding to p-Tyr-14-Cav-1 affects eNOS activity. Nitrite (NO_2^-, the stable product of NO autoxidation) concentration was measured in media from HEK cells stably expressing WT-eNOS (Supplemental Figure S5) following transient transfection with WT-Cav-1-YFP, Y14D-Cav-1-YFP, and Y14F-Cav-1-YFP as before. Cells were then treated with 5 μM A23187 for 30 min. Compared to HEK/eNOS cells, cells transfected with WT-Cav-1-YFP showed 31% less NO production (1.00 ± 0.021 vs. 0.693 ± 0.029 R.U.; $p < 0.001$; n = 8). Furthermore, accumulated NO_2^- in cell culture media was 40% less in HEK/eNOS cells transfected with Y14D-Cav-1 mutant than in WT-Cav-1–expressing cells (Figure 4C). To determine the effect of Y14D-Cav-1 on eNOS activity, NO_2^- production per minute per 10^6 HEK/eNOS cells transfected with WT-Cav-1-YFP, Y14D-Cav-1-YFP, and Y14F-Cav-1-YFP mutants was calculated from serial samples. A23187-induced eNOS activation was maximal after 1 min, returned to near basal activity at 3 min, and then remained low at all later time points (Figure 4D), which was similar to the time course of NO generation observed in HUVECs (Supplemental Figure S1B). Importantly, these data indicate that Y14D-Cav-1 limits A23187-stimulated eNOS activation compared with cells expressing an equivalent level of WT-Cav-1 or phosphodefective Y14F-Cav-1.

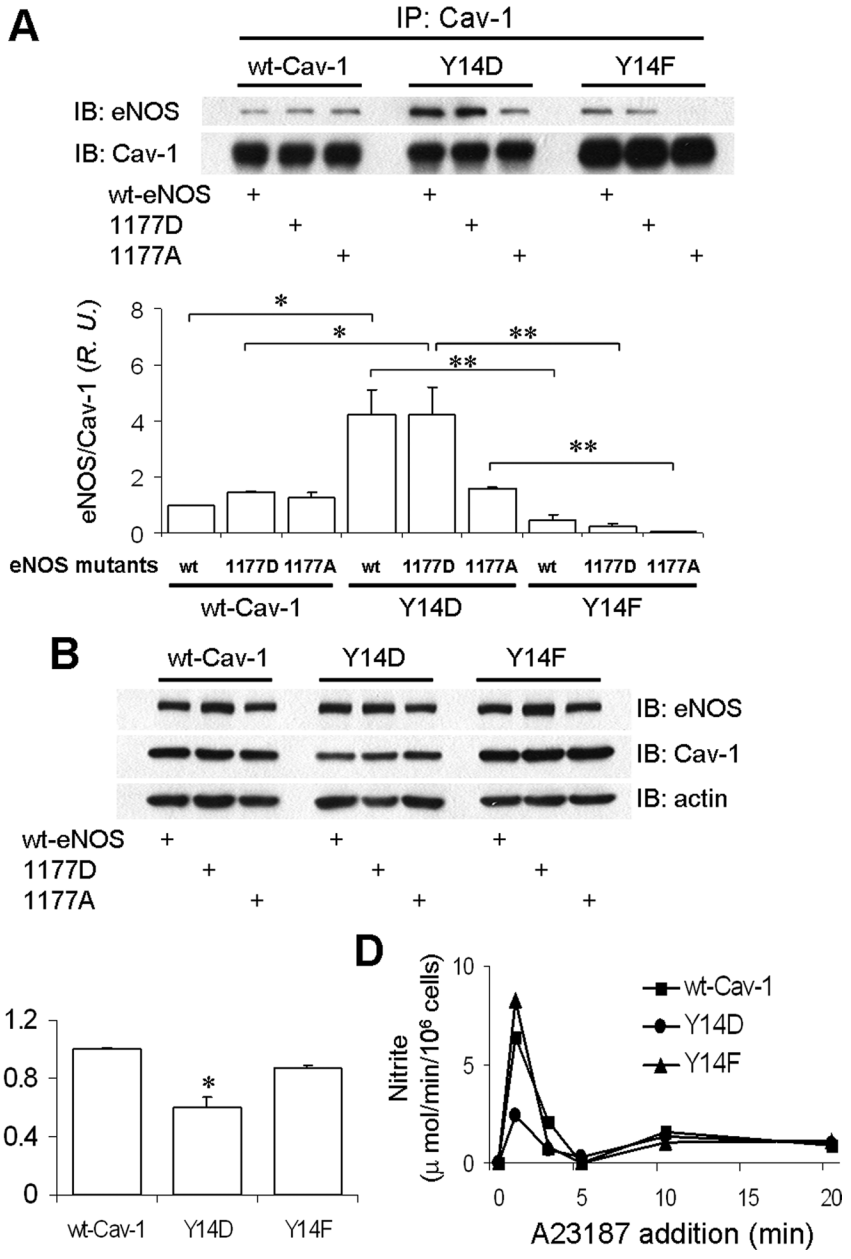

FIGURE 4: Binding of Y14D-Cav-1 with eNOS inhibits eNOS activity. (A) CoIP of Cav-1 and eNOS mutants in HEK cells. WT-eNOS-CFP, eNOS-S1177D-CFP, and eNOS-S1177A-CFP were transiently transfected in HEK cells stably expressing WT-Cav-1-YFP, Cav-1-Y14D-YFP, or Cav-1-Y14F-YFP. Cell lysates were immunoprecipitated with anti–Cav-1 pAb 48 h after transfection of eNOS mutants in the absence of stimulation. Ratio of WT-eNOS-CFP/wt-Cav-1-YFP was set at 1 (*$p < 0.05$; **$p < 0.005$). Bar graph shows mean ± SEM (n = 3). (B) Protein levels of Cav-1 and eNOS mutants in transfected HEK cells before IP. (C) Nitrite accumulation in HEK/eNOS cells transiently transfected with Cav-1 mutant cDNAs (mean ± SEM; n = 11). Cells were treated for 30 min with 5 μM A23187, and supernatants were collected for nitrite assay (*$p < 0.001$). (D) eNOS activity (representative of four independent experiments) of stable HEK/eNOS cells transiently transfected with Cav-1 mutants.

times indicated (Figure 5A). eNOS protein expression was significantly reduced after eNOS siRNA treatment. In addition, the basal p-Tyr-418-Src level was reduced by 50% in eNOS-depleted cells and remained low up to 10 min after addition of A23187 compared with scrambled siRNA-treated cells (Figure 5A). Thus, p-Src was significantly lower at each time point in eNOS siRNA–treated HUVECs compared with scrambled siRNA–treated HUVECs, suggesting that NO production by eNOS in response to Ca^{2+} increases Src activity. We speculate that residual Src activation may be due to nNOS-derived NO (Bachetti *et al.*, 2004).

Consistent with this finding, p-Tyr-14-Cav-1 induced by A23187 stimulation was also significantly reduced in HUVECs treated with eNOS siRNA (Figure 5A). Thus eNOS and NO production lie upstream of Src activation and Cav-1 phosphorylation. In other experiments, Cav-1–null mouse embryonic fibroblasts (MEFs) were stimulated with 0.2 mM DEA NONOate, an NO donor, and lysates were probed for p-Tyr-418-Src. As shown in Figure 5B, NO donor increased Src activity by 80% compared with nontreated cells, in accord with the finding that eNOS expression is an important determinant of Src activation. In WT MEFs stimulated with DEA-NONOate, we observed a 50% increase in pTyr-418-Src, and thus 37% less Src activation than observed in WT MEFs, consistent with the idea that phosphor–Cav-1 plays an important role in the mechanism of Src inactivation (Cao *et al.*, 2002; Place *et al.*, 2011).

To further address the role of NO signaling in the mechanism of Src activation, WT-HEK cells and HEK cells stably expressing eNOS were stimulated with A23187. As shown by Western blotting, we observed a 66% increase in Src-Tyr-418 phosphorylation in eNOS-expressing HEK cells treated for 5 min with A23187 compared with WT-HEK cells lacking eNOS (Figure 5C; n = 7, $p < 0.001$). NO activation of Src was also determined using a Src FRET biosensor (Figure 5D), which is composed of CFP, the Src SH2 domain, a flexible linker, a Src substrate peptide, and YFP (Wang *et al.*, 2005). On Src activation, CFP moves away from YFP and FRET decreases. eNOS-expressing HEK cells transiently transfected with the biosensor were imaged by confocal microscopy (a typical FRET image is shown in Figure 5D). After stimulation with 5 μM A23187, CFP intensity increased, whereas as that of YFP decreased, indicating CFP movement away from YFP and thus evidence of increased Src kinase activity. Src kinase activity indicated by FRET was blocked by L-NAME and PP2 (Figure 5E). As a negative control,

NO-mediated Src activation stimulates Cav-1 Tyr-14 phosphorylation

We next addressed the possibility that eNOS-derived NO can itself activate Src and mediate tyrosine phosphorylation of Cav-1 needed for the inhibitory Cav-1 interaction with eNOS. In this experiment, we depleted eNOS in HUVECs with small interfering RNA (siRNA) and measured Src activation. eNOS siRNA (100 nM) was added to HUVECs, and after 72 h, cells were treated with 5 μM A23187 for the

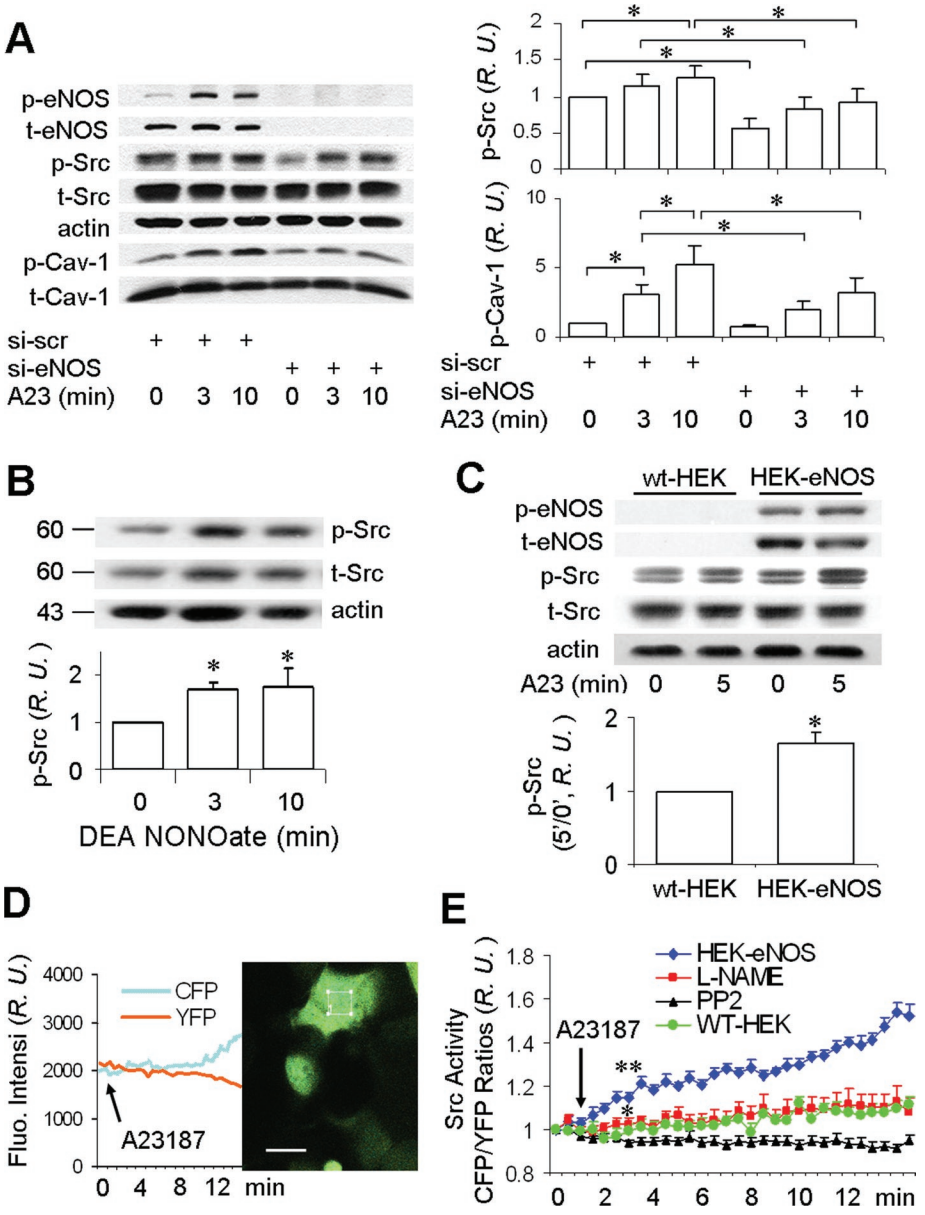

FIGURE 5: NO-dependent Src activation mediates Cav-1–Tyr-14 phosphorylation. (A) Decreased phosphorylation of Src–Tyr-418 and Cav-1–Tyr-14 in HUVECs after eNOS siRNA treatment (mean ± SEM; n = 4). Ratio of phosphorylated to total protein at 0 min was set at 1 (*p < 0.05). (B) The NO donor DEA NONOate induces Src activation in Cav-1–null MEF cells (mean ± SEM; n = 3). After stimulation with 0.2 mM DEA NONOate at indicated times, cells were prepared for Western blotting (*p < 0.05). (C) eNOS/NO-dependent Src activation in HEK cells (mean ± SEM; n = 7). The ratio of p-Tyr-418-Src at 5 min of A23187 treatment vs. untreated in WT-HEK cells was set as 1 (*p < 0.001 vs. WT-HEK). (D) A typical live-cell FRET image of HEK/eNOS cells expressing Src FRET biosensor. Fluorescence intensity of CFP and YFP was measured in the ROI (white box) before and after treatment with 5 μM A23187. Bar, 10 μm. (E) Activation of Src measured by FRET in HEK/eNOS cells expressing Src-FRET biosensor (mean ± SEM; n = 13). After cells were pretreated with medium alone, 1 mM L-NAME, or 15 μM PP2 for 30 min at 37°C, 5 μM A23187 was added and FRET was measured (*p < 0.05 vs. WT-HEK cells; **p < 0.01 all times beyond 2 min after A23187 addition vs. 0 min).

Src kinase activity determined in WT-HEK cells (lacking eNOS) showed no change in the Src FRET signal following stimulation with A23187 (Figure 5E). These results show that eNOS-derived NO activates Src kinase, which phosphorylates Cav-1, leading to increased eNOS binding to Cav-1 and inhibition of eNOS activity.

Proposed mechanism of NO-dependent negative feedback inhibition of eNOS

Data shown here indicate that stimulation of endothelial cells with calcium ionophore A23187, thrombin, or VEGF induces eNOS activation and NO-dependent Src activation. We also observed Cav-1 phosphorylation and enhanced binding between phospho-Cav-1 and eNOS, which was associated with a decrease in eNOS activity. Thus, as summarized in Figure 6, we propose a mechanism in which phospho–Cav-1 binding to eNOS decreases eNOS activity. The proposed negative feedback mechanism is supported by experimental data that show that eNOS–Cav-1 interactions (coIP and FRET) are blocked by eNOS inhibitor L-NAME and Src inhibitor PP2 and that phosphomimicking mutants rather than phosphodefective Cav-1 and eNOS mutants specifically bind to each other. NO and Src-dependent phosphorylation of Cav-1 therefore may be a primary mechanism of eNOS negative feedback regulation in endothelial cells.

DISCUSSION

Here we demonstrate a novel phospho-Cav-1–dependent mechanism of eNOS/Cav-1 binding that mediates eNOS inactivation. eNOS-derived NO production increased Src activity and subsequently the phosphorylation of Cav-1 Tyr-14 in endothelial cells, which promoted the binding of eNOS and Cav-1. Thus these data suggest NO production per se negatively regulates eNOS activity secondary to Cav-1 Tyr-14 phosphorylation. The association between eNOS and Cav-1, as assessed by coIP of endogenous and expressed proteins, was enhanced by Cav-1 Tyr-14 phosphorylation and phosphomimicking Y14D Cav-1 mutant and blocked by L-NAME, Src inhibitor PP2, and Y14F phosphodefective mutant. FRET analysis of Cav1-YFP and eNOS-CFP, together with measures of Ca^{2+}-induced NO production, support the hypothesis that p-Tyr-14-Cav-1 provides a favorable conformation for CSD-dependent binding of phosphorylated eNOS, resulting in inhibition of eNOS activity. Of interest, in additional studies we observed that depletion of Cav-1 from human endothelial cells with siRNA-enhanced Ca^{2+}-induced eNOS activation (unpublished data). However, we also noted decreased eNOS protein level in Cav-1 siRNA-treated cells, suggesting that Cav-1 may stabilize eNOS and prevent degradation. The mechanism by which Cav-1 serves to regulate eNOS expression/stability and whether Cav-1 phosphorylation also plays a role in this process require further investigation.

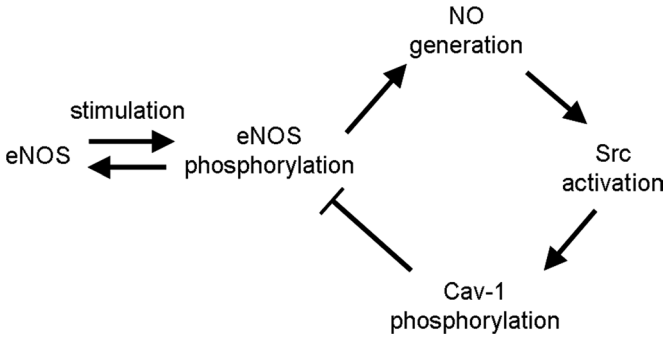

FIGURE 6: Proposed mechanism of negative feedback regulation of eNOS by phospho–Cav-1. Ca^{2+}-dependent stimulation of endothelial cells induces eNOS activation by phosphorylation on Ser-1177, and NO is released within 1 min. NO induces Src activation and phosphorylation of Cav-1 on Tyr-14, which we propose leads to unmasking of the caveolin scaffolding domain. Phosphorylated Cav-1 then binds to activated eNOS, inhibiting eNOS activity, and release of NO, thus returning eNOS to its basal state. eNOS/Cav-1 interaction can be blocked by eNOS inhibitor L-NAME and Src inhibitor PP2, suggesting that an NO/Src-dependent feedback mechanism mediates eNOS inactivation.

NO is a well-established signaling molecule and key regulator of cardiovascular function (Furchgott and Zawadzki, 1980; Huang *et al.*, 1995). Tight control of NO production is believed to be critically important for maintenance of cellular and tissue homeostasis. The importance of Cav-1, the primary coat protein of caveolae, in the regulation of eNOS activity and NO production has been studied in recent years. eNOS localized to the inner leaflet of caveolar membranes and in the Golgi in endothelial cells is believed to be held in an inactive state due to direct interaction with Cav-1 (Frank *et al.*, 2003; Gratton *et al.*, 2004).The binding of eNOS to Cav-1 maintains eNOS in its inactive conformation, whereas CaM binding increases eNOS activity (Michel *et al.*, 1997a, 1997b; Gratton *et al.*, 2004; Ju *et al.*, 1997). eNOS contains a consensus caveolin-binding motif located within amino acids 348–356 (García-Cardeña *et al.*, 1997; Smart *et al.*, 1999; Couet *et al.*, 1997), and Cav-1 overexpression in COS-7 cells decreases eNOS activity (García-Cardeña *et al.*, 1997), consistent with the essential role of Cav-1 in restraining eNOS activity. Several studies have also shown increased NO production in *Cav1*$^{-/-}$ mice and that disruption of the eNOS–Cav-1 complex leads to increased eNOS activity and prolonged NO release, which has been linked to tissue and organ pathologies (Drab *et al.*, 2001; Zhao *et al.*, 2002; Wunderlich *et al.*, 2006; Maniatis *et al.*, 2008; Razani *et al.*, 2001). Whether Cav-1 plays a role specifically in the mechanism of eNOS *inactivation* has not been established.

We addressed the mechanism regulating interaction of eNOS with Cav-1 following Ca^{2+}-, VEGF-, and thrombin-induced eNOS activation. Cells were treated with agonists to stimulate a rise in intracellular Ca^{2+} concentration, which was shown to induce eNOS activation and production of NO (Jin, 2006). We observed Src kinase activation downstream of NO generation, which has been ascribed to S-nitrosylation of Src at Cys-498 (Raman *et al.*, 1998). The resultant phosphorylation of eNOS Ser-1177 and Cav-1 Tyr-14 increased eNOS/Cav-1 binding, which was associated with a decrease in eNOS activity. This was evident from results showing that WT-Cav-1 interacted equally well with WT-eNOS and with phosphomimicking or phosphodefective eNOS mutants expressed in HEK cells, whereas the phosphomimicking Cav-1 mutant (Cav-1-Y14D) interacted strongly with WT-eNOS and phosphomimicking eNOS but not with phosphodefective eNOS. In contrast, phosphodefective Cav-1 mutant (Cav-1-Y14F) failed to interact with any of the eNOS variants. The results of these phosphomimicking and phosphodefective Cav-1 and eNOS mutant–binding studies, even with the potential caveat that these mutants simply mimic the presence or absence of the negatively charged phosphate residue, are consistent with that observed with endogenous proteins in the absence and presence of Src kinase inhibitor. Our conclusion from these studies is that Cav-1 phosphorylation at Tyr-14 provides the most favorable conformation for eNOS binding and inhibition of eNOS activity.

Ca^{2+}-calmodulin activates eNOS, and high concentration of CaM (1 μM) can prevent eNOS/Cav-1 binding in vitro (Bernatchez *et al.*, 2011). In the present studies, we observed stimulation- and time-dependent increase in CaM coIP with eNOS following addition of Ca^{2+} ionophore A23187 (Supplemental Figure S3). In this same experiment we observed an increase in the amount of Cav-1 that coimmunoprecipitated with eNOS. Data in the literature demonstrate inhibition of eNOS-derived NO production by Cav-1 or Cav-1 scaffold domain peptide that can be completely reversed by CaM (Ghosh *et al.*, 1998). However, it has not been shown to our knowledge that CaM binding to eNOS promotes release of Cav-1 from eNOS. Similarly, whereas addition of Cav-1 or Cav-CSD decreases eNOS activity, CaM was not shown to be displaced from eNOS (Raman *et al.*, 1998). Thus, since eNOS has separate binding sites for CaM (amino acids [aa] 491–510; Michel *et al.*, 1997b) and Cav-1 (aa 348–356; Couet *et al.*, 1997), data presented here indicate that activation of CaM and phosphorylation of Cav-1 increase their binding to eNOS. In both cases, the binding of either CaM or Cav-1 to eNOS is believed to induce a conformational change in the eNOS heme-domain activation motif (aa 96–101; Raman *et al.*, 1998).

A distinct feature of these studies was that we monitored interactions between eNOS and Cav-1 by both FRET and coIP. For the latter, we used the total membrane fraction (containing virtually 100% of the total eNOS and Cav-1 protein) instead of membrane-enriched fractions that contain only a small amount of the total eNOS (Supplemental Figure S2). Of interest, coIP of endogenous eNOS and Cav-1 from HUVEC total cell lysates increased upon Ca^{2+}-dependent stimulation, peaking ~5 min after treatment with A23187. In transfected CHO cells, eNOS–Cav-1 binding also increased upon stimulation with A23187 or thrombin, as shown by coIP and FRET. Similarly, we observed increased interaction between eNOS and Cav-1 in mouse lungs, indicating the physiological relevance of the cell observations describing the basis of the interaction of eNOS with phospho–Cav-1.

A key question that arose from our studies relates to the mechanism of NO-induced Src activation and thereby Cav-1 phosphorylation on Tyr-14. In HUVECs in which eNOS was depleted by siRNA treatment, we observed significantly reduced phosphorylation of Src and Cav-1 in response to A23187, in contrast to control cells. It is possible that nNOS may be responsible for residual Src activation observed in eNOS siRNA or L-NAME–treated cells, as this isoform is also expressed in endothelial cells and believed to account for up to 20% of Ca^{2+}-induced NO release (Bachetti *et al.*, 2004). Furthermore, Src FRET biosensor experiments showed that phosphorylation and activation of eNOS by addition of A23187 stimulated Src activity, which was inhibited by the pharmacological Src inhibitor PP2, as well as by eNOS inhibitor L-NAME. Moreover, NO derived from an exogenous source, DEA NONOate, induced Src activation, consistent with previous reports (Akhand *et al.*, 1999; Monteiro *et al.*, 2000) and evidence that NO-mediated S-nitrosylation of Src Cys-498 increases Src kinase activity (increase in Src p-Tyr-418) in a dose-dependent manner (Raman *et al.*, 1998). It should be noted

here that phosphorylated Cav-1 also functions as a negative regulator of Src activity by facilitating the recruitment of C-terminal Src kinase (Csk), which is known to phosphorylate Src-negative regulatory Tyr-529 and induce Src inactivation (Place *et al.*, 2011).

The functional significance of Cav-1 Tyr-14 phosphorylation was previously linked to tumor cell migration (Joshi *et al.*, 2008), modulation of focal adhesion (Grande-García *et al.*, 2007), mechanotransduction (Radel *et al.*, 2007), and caveolae formation and endocytosis (Minshall *et al.*, 2000; Shajahan *et al.*, 2004; Orlichenko *et al.*, 2006; Hu *et al.*, 2006, 2008; Sverdlov *et al.*, 2007, 2009; Sun *et al.*, 2009). Data presented here indicate that pTyr-14-Cav-1 may obtain a favorable conformation that leads to enhanced docking of proteins, presumably via the CSD, thus enabling recruitment of proteins to caveolae, where signaling can be regulated. We posit that a negative feedback mechanism that returns eNOS activity to its ground state may be pathophysiologically important in vascular inflammation, which is often associated with dysregulated eNOS activity, persistent NO production, and NO modification of endothelial regulatory proteins (Siddiqui *et al.*, 2011).

MATERIALS AND METHODS

Cell culture and transfection

HUVECs were purchased from Vec Technologies (Rensselaer, NY). Cav-1–null and WT mouse embryonic fibroblasts, HEK 293, and CHO-K1 cells were from the American Type Culture Collection (Rockville, MD). HUVEC growth medium (EGM-2 plus Bullet kit) was from Lonza (Walkersville, MD). Nitrocellulose membrane was from Bio-Rad Laboratories (Hercules, CA). Supersignal West Femto Kit and Restore Western Stripping buffer were from Pierce (Rockford, IL). HAM's F-12 (for CHO cells) and DMEM (for HEK 293 cells and MEFs) were from Invitrogen (Grand Island, NY). Fetal bovine serum (FBS) was from Serum Source International (Charlotte, NC). Geneticin was purchased from Invitrogen (Carlsbad, CA). The 96-well assay plate for NO measurement was from Corning (Corning, NY).

HUVECs were cultured in EGM-2 medium (Lonza) supplemented with 10% (vol/vol) FBS, split 1:4 upon reaching confluence, and used at passages 5–7. For immunofluorescence microscopy, cells were grown on noncoated glass coverslips. For DAF-2 DA experiments, cells were grown in black, clear-bottom, 96-well plates (Costar, Acton, MA,). CHO cells were cultured in Ham's F-12 medium supplemented with 10% FBS and 1% penicillin/streptomycin. HEK 293 and MEF cells were cultured in DMEM supplemented with 10% FBS and 1% penicillin/streptomycin. cDNAs of Cav-1 or eNOS mutants were transfected in CHO or HEK 293 cells using Lipofectamine 2000 (Invitrogen) according to the manufacturer's instructions. Cells were selected with Geneticin 24–36 h after transfection. Stable cell lines were obtained by fluorescence-activated cell sorting plating and growth of single cells in 96-well plates in presence of Geneticin. Cells transduced with fluorescently tagged proteins were verified by fluorescence microscopy and immunoblot analysis.

Reagents

PP2, A23187 (calcimycin), L-NAME, and H89 were from Sigma-Aldrich (St. Louis, MO). Human α-thrombin was from Enzyme Research Laboratories (South Bend, IN). 4,5-DAF-2 DA, 5-iodotubercidin, and STO-609 were from Calbiochem (La Jolla, CA). Recombinant human VEGF-165 was from Shenandoah Biotechnology (Warwick, PA). Glass-bottom dishes for live-cell images were from MatTek (Ashland, MA). DEA NONOate was from A.G. Scientific (San Diego, CA). *n*-Octyl-β-D-glucopyranoside (ODG) was from RPI Corp. (Mt. Prospect, IL). siRNA of eNOS and transfection reagent DharmaFect 1 were from Dharmacon (Lafayette, CO). DAPI, Lipofectamine 2000, mammalian expression vectors pcDNA3 and pcDNA6, and Geneticin were purchased from Invitrogen (Carlsbad, CA). The vectors for CFP and YFP were obtained from Clontech (Palo, Alto, CA). Mouse anti-eNOS, rabbit anti–caveolin-1, mouse anti–Tyr-14-caveolin-1, rabbit and mouse immunoglobulin G, and mouse anti-actin were from BD Biosciences (San Diego, CA). Rabbit anti–phospho-Tyr-418-Src, rabbit anti-eNOS, rabbit anti–phospho-Ser-1177-eNOS, rabbit anti–phospho-Ser-473-Akt, and rabbit anti–phospho-Thr-308-Akt were from Cell Signaling Technology (Danvers, MA). Rabbit anti–c-Src and anti-AKT antibodies were from Santa Cruz Biotechnology (Santa Cruz, CA). Mouse anti-CaM was from Millipore (Temecula, CA).

Construction of Cav-1-YFP, Cav-1-Y14D-YFP, and Cav1-Y14F-YFP plasmids

To generate the wild-type, C-terminal, YFP-tagged caveolin-1 (Cav-1-YFP), full-length *Homo sapiens* Cav-1 was used as a template in a PCR with DNA Phusion High-Fidelity Polymerase (New England BioLabs, Ipswich, MA), using the following primer pair lacking the stop codon: Cav1-WT-F:5′-ACTA*GCTAG C*GACCGCCATGTCTGGGGGCAAAT-AC-3′ and Cav-1-WT-R:5′-ACTG*GGTACC*GTTATTTC-TTTCTGCAAGTTGATGCG-3′. The resulting PCR fragment was digested with restriction enzymes 5′-*Nhe*I and 3′-*Kpn*I (italicized in the primers) and subcloned into pEYFP-N1 vector (Clontech, Mountain View, CA).

To generate the Cav-1-Y14D-YFP plasmid, a two-step PCR method was used. In the first step, two PCR fragments were generated using the wild-type caveolin 1 cDNA as the DNA template and the following primer pairs: fragment A, primer pairs Cav-1-WT-F and Cav-1-Y14D-R-5′-ATGGGAACGGTGTCGAGATGTCC-3′, and fragment B, primer pairs Cav-1-Y14D-R-5′-ATGGGAACGGTGTCGAGATGTCC-3′ and Cav-1-WT-R. As shown in the primers, the underlined base pair resulted in Y14-to-D14 mutation. In the second step, a final PCR product, fragment C, was generated by combining fragments A and B together as PCR DNA templates with primer pair Cav-1-WT-F and Cav-1-WT-R. The fragment C was digested with *Nhe*I and *Kpn*I ligated at the same restriction sites of pEYFP-N1 vector.

Similar to the Y14D plasmid, the Cav-1-Y14F-YFP plasmid was generated in the first PCR step using primer pairs for fragment A, Cav-1-WT-F and Cav-1-Y14F-R-5′-ATGGGAACGG-TAAAGAGATGTCC-3′, and Cav-1-Y14F-F-5′-GGACATCTCTTTACCGT-TCCCAT-3′ and Cav1-WT-R for fragment B. Fragment C was generated with primer pairs Cav-1-F and Cav-1-R and both fragments A and B as DNA templates. Fragment C was digested and ligated as described. All resulting plasmids were verified and analyzed by gel analysis and sequencing analysis.

Construction of pcDNA3-eNOS-CFP, pcDNA3-eNOS-S1177D-CFP, and pcDNA3-eNOS-S1177A-CFP plasmids

The 5′-*Nhe*I/3′-*Sma*I fragment of CFP from pECFP-C1 (Clontech) was subcloned into pACGp67A (BD Biosciences) at the 5′-*Xba*I/3′-*Eco*RI sites, creating pACGp67A-CFP. The CFP fragment was then excised at 5′-*Bam*HI/ 3′-*Not*I sites from the pACGp67A-CFP and ligated at the same restriction sites into pcDNA3 (Invitrogen), creating pCDNA3-CFP. To create the vector eNOS with CFP tagged at the C-terminus, full-length *H. sapiens* eNOS cDNA (with GenBank Accession number NM_000603 from OriGene Technologies, Rockville, MD) was used as DNA template in a PCR to generate eNOS PCR fragment that contained *Age*I at both 5′ and 3′ ends. The 5′/3′-*Age*I fragment of eNOS was then digested and ligated to the same restriction sites on the pcDNA3-CFP vector to create the pcDNA3-eNOS-CFP plasmid. The primers used were eNOS-AgeI-F,

5′-ATTATA*ACCGGT*AGCCACCATGGGCAACTTGAAG-AG-3′; and eNOS-NoSTOP-AgeI-R, 5′-ATTATA*ACCGGT*AGGGGGCTGTTGGT-GTCTGAG-3′.

For the mutation of serine 1177 in eNOS, a two-step PCR method was used. In the first step, two PCR fragments were generated by PCR using eNOS cDNA as DNA template. For the generation of pCDNA3-eNOS-S1177D-CFP plasmid, the following primers were used: for fragment A, primer pair eNOS-AgeI-F and eNOS-S1177D-R:5′-CTGACGCTCCTGCAAG-TCAAAGCTC-TG-3′; for fragment B, primer pair, eNOS-S1177D-F:5′-TACGCACCCAGA-GCTTTGACTT-GCAGGAG-3′ and eNOS-NoStop-AgeI-R. Underlined base pairs indicated sites of amino acid point mutation. In the second step, a final PCR product, fragment C, was generated by combining fragments A and B together as PCR DNA templates with primer pair eNOS-AgeI-F and eNOS-NoSTOP-AgeI-R. PCR fragment C was then digested and ligated as described to create pCDNA3-eNOS-S1177D-CFP plasmid.

Similarly, the pCDNA-eNOS-S1177A-CFP plasmid was generated in the first PCR step using primer pairs for fragment A, eNOS-AgeI-F and eNOS-S1177A-R:5′-CTGACGCTCCT-GCAAGGCAAA-GCTCTG-3′; and for fragment B, eNOS-S1177A-F:5′-TACGCACC-CAGA-GCTTTGCCTTGCAGGAG-3′ and eNOS-NoStop-AgeI-R. Fragment C was generated with primer pair eNOS-AgeI-F and eNOS-NoStop-AgeI-R using both fragments A and B as DNA templates. The resulting PCR fragment C was also digested and ligated as described, creating pCDNA-eNOS-S1177A-CFP plasmid. All generated plasmids were verified and analyzed by gel analysis and sequencing analysis.

Analysis of eNOS activity by DAF-2 fluorescence

Intracellular NO measurement using the NO-specific fluorescence probe DAF-2 DA was described previously (Nakatsubo *et al.*, 1998; Kojima *et al.*, 1998). Briefly, after incubation in serum-free EGM-2 (containing 0.1% BSA) overnight, endothelial cells on 96-well plates were washed with Krebs–Ringer phosphate (KRP) buffer (120 mM NaCl, 4.8 mM KCl, 0.54 mM $CaCl_2$, 1.2 mM $MgSO_4$, 11 mM glucose, 15.9 mM sodium phosphate, pH 7.20), incubated with 5 μM DAF-2 DA in KRP buffer for 30 min at room temperature, washed again with KRP buffer, and then incubated with KRP buffer for 30 min at 37°C in the absence or presence of 1 mM L-NAME, after which calcium ionophore A23187, thrombin, VEGF, or KRP buffer was added to the wells. Fluorescence (emission wavelength, 485 nm; excitation wavelength, 538 nm) was measured temporally at 37°C from 0 to 60 min using the bottom-reading mode in a FlexStation II plate reader (Molecular Devices, Sunnyvale, CA). DAF-2 DA experiments were repeated at least three times, and eight wells were used in each experiment.

Chemiluminescence-based NO measurements

HUVECs were washed twice with HBSS and incubated with HBSS-Arg (HBSS plus 0.2–0.5 mM L-arginine) for 30 min at 37°C. The cells were then treated with agonists for up to 30 min in HBSS-Arg. NO concentration in the culture media was assessed by measuring NO_2^- accumulation as described (Bonini *et al.*, 2002), using a Sievers NO Analyzer (Sievers Instruments, Boulder, CO). NO release from transfected HEK cells was assessed from NO_2^- level in the media (Michel *et al.*, 1997a; Bernatchez *et al.*, 2005) and reported as μmol NO_2^-/min per 10^6 cells.

Fluorescence resonance energy transfer

Cells cultured on glass-bottom dishes were imaged with a Zeiss LSM-510 META confocal microscope (Carl Zeiss, Jena, Germany) as described previously (Chen *et al.*, 2006). Two images of the basal fluorescence were collected before addition of stimulus. Intensity of donor and acceptor emission was determined from selected ROIs and was averaged and plotted as acceptor/donor (YFP/CFP) as an index of Src biosensor activity (Wang *et al.*, 2005) or donor/acceptor (CFP/YFP) to reflect temporal changes in eNOS/Cav-1 FRET.

siRNA-mediated eNOS depletion

Confluent HUVECs seeded in 35-mm wells were grown to ~40% confluence and transfected with eNOS or scrambled siRNA at a final concentration of 100 nM. After 72 h, cells were stimulated and lysed for Western blot analysis.

Immunoprecipitation and Western blotting

After treatment with different reagents, cells were lysed by sonication in 2% ODG in Tris buffer (pH 7.50, 50 mM Tris, 150 mM NaCl, 1 mM NaF, 1 mM EDTA, 1 mM Na_3VO_4, 44 μg/ml phenylmethylsulfonyl fluoride [PMSF], 1% protease inhibitor cocktail). The lysates were centrifuged for 20 min at 16,000 × *g* at 4°C. Supernatants were collected for IP or Western blot analysis. For IP, antibodies were added to the cell lysates in 1.5-ml Eppendorf tubes and rotated overnight at 4°C and then rotated for 2 h at 4°C with protein A beads. The beads were washed five times with Tris buffer containing 1% ODG. The proteins were eluted with Laemmli buffer, subjected to SDS-PAGE, transferred to nitrocellulose membranes, and probed with primary and secondary antibodies. Membrane-bound antibodies were visualized using Supersignal West Femto Kit.

Phosphorylation of eNOS (Ser-1177), Src (Tyr-418), Cav-1 (Tyr-14), and Akt (Thr-308, Ser-473) after stimulation with A23187

After serum deprivation in culture medium containing 0.5% FBS overnight or 0.1% FBS for 5–7 h, cells were washed three times with serum-free medium. Agonists were added to the cells at indicated times and incubated at 37°C. For inhibitor experiments, inhibitors were added 30 min prior to stimulation. Finally, after washing once with ice-cold Tris buffer (50 mM Tris, 150 mM NaCl, 1 mM NaF, 1 mM EDTA, 1 mM Na_3VO_4, 44 μg/ml PMSF, pH 7.50), the cells were collected and lysed for Western blotting or IP.

Comparison of membrane fractions for coIP experiment in HUVECs

Membrane-enriched fractions of HUVEC were prepared for coIP as described (Busconi and Michel, 1993; Feron *et al.*, 1998), but with the following modifications. Briefly, after treatment with vehicle or 5 μM A23187 for 3 min at 37°C, cells were collected and sonicated in phosphate-buffered saline (containing 1% protease inhibitor cocktail) and centrifuged at 100,000 × *g* for 30 min at 4°C. The supernatants (cytosolic fraction) were collected, and pellets were dissolved in 2% ODG in Tris buffer and centrifuged again for 30 min at 100,000 × *g*. The supernatants (membrane-enriched fraction) were collected and the pellets were dissolved in RIPA buffer (150 mM NaCl, 1.0% IGEPAL CA-630, 0.5% sodium deoxycholate, 0.1% SDS, and 50 mM Tris, pH 8.0) by sonication. Insoluble fractions after ODG were collected by centrifugation for 10 min at 1000 × *g*. For isolation of the total membrane fraction, cells were dissolved in 2% ODG (Tris buffer) by sonication, and supernatants (total membrane fraction) were collected after centrifugation for 20 min at 16,000 × *g*. The pellets were then dissolved by sonication in RIPA buffer. Supernatants (insoluble fractions in ODG) were cleared by centrifugation for 10 min at 1000 × *g*, and then all fractions were prepared for immunoblotting or IP.

Mouse lung preparations

Anesthetized mice were killed and lungs perfused via pulmonary artery cannula with DMEM/F-12 medium (without FBS) for 10 min at 0.2 ml/min at 37°C. Lungs were then perfused with medium containing 5 µM A23187 for 0, 3, and 10 min and then rinsed with cold medium containing phosphatase inhibitors for another 3 min. Lungs were homogenized and sonicated in Tris buffer containing 2% ODG. Lysates were centrifuged for 20 min at 16,000 × *g* at 4°C, and supernatants were collected for immunoblotting or IP.

Statistical analysis

Data are expressed as mean ± SEM. Statistical analysis was performed by Student's *t* test or one-way analysis of variance using Graph InStat software (San Diego, CA).

ACKNOWLEDGMENTS

We thank Maricela Castellon for technical assistance, William Sessa for providing eNOS cDNA, and Shu Chien for providing the Src FRET biosensor cDNA. This work was supported by National Institutes of Health National Heart, Lung, and Blood Institute Grants R01 HL045638, R01 HL71626, and P01 HL60678.

REFERENCES

Akhand AA, Pu M, Senga T, Kato M, Suzuki H, Miyata T, Hamaguchi M, Nakashima I (1999). Nitric oxide controls src kinase activity through a sulfhydryl group modification-mediated Tyr-527-independent and Tyr-416-linked mechanism. J Biol Chem 274, 25821–25826.

Atochin DN, Huang PL (2010). Endothelial nitric oxide synthase transgenic models of endothelial dysfunction. Pflugers Arch 460, 965–974.

Bachetti T, Comini L, Curello S, Bastianon D, Palmieri M, Bresciani G, Callea F, Ferrari R (2004). Co-expression and modulation of neuronal and endothelial nitric oxide synthase in human endothelial cells. J Mol Cell Cardiol 37, 939–45.

Bernatchez PN, Bauer PM, Yu J, Prendergast JS, He P, Sessa WC (2005). Dissecting the molecular control of endothelial NO synthase by caveolin-1 using cell-permeable peptides. Proc Natl Acad Sci USA 102, 761–766.

Bernatchez P, Sharma A, Bauer PM, Marin E, Sessa WC (2011). A noninhibitory mutant of the caveolin-1 scaffolding domain enhances eNOS-derived NO synthesis and vasodilation in mice. J Clin Invest 121, 3747–3755.

Bonini MG, Mason RP, Augusto O (2002). The mechanism by which 4-hydroxy-2,2,6,6-tetramethylpiperidene-1-oxyl (tempol) diverts peroxynitrite decomposition from nitrating to nitrosating species. Chem Res Toxicol 15, 506–511.

Bucci M, Gratton JP, Rudic RD, Acevedo L, Roviezzo F, Cirino G, Sessa WC (2000). In vivo delivery of the caveolin-1 scaffolding domain inhibits nitric oxide synthesis and reduces inflammation. Nat Med 6, 1362–1367.

Busconi L, Michel T (1993). Endothelial nitric oxide synthase. N-Terminal myristoylation determines subcellular localization. J Biol Chem 268, 8411–8413.

Cao H, Courchesne WE, Mastick CC (2002). A phosphotyrosine-dependent protein interaction screen reveals a role for phosphorylation of caveolin-1 on tyrosine 14: recruitment of C-terminal Src kinase. J Biol Chem 277, 8771–8774.

Chen Z, Deddish PA, Minshall RD, Becker RP, Erdös EG, Tan F (2006). Human ACE and bradykinin B2 receptors form a complex at the plasma membrane. FASEB J 20, 2261–2270.

Couet J, Li S, Okamoto T, Ikezu T, Lisanti MP (1997). Identification of peptide and protein ligands for the caveolin-scaffolding domain. Implications for the interaction of caveolin with caveolae-associated proteins. J Biol Chem 272, 6525–6533.

Drab M *et al*. (2001). Loss of caveolae, vascular dysfunction, and pulmonary defects in caveolin-1 gene-disrupted mice. Science 293, 2449–2452.

Dudzinski DM, Michel T (2007). Life history of eNOS: partners and pathways. Cardiovasc Res 75, 247–260.

Feron O, Belhassen L, Kobzik L, Smith TW, Kelly RA, Michel T (1996). Endothelial nitric oxide synthase targeting to caveolae. Specific interactions with caveolin isoforms in cardiac myocytes and endothelial cells. J Biol Chem 271, 22810–22814.

Feron O, Michel JB, Sase K, Michel T (1998). Dynamic regulation of endothelial nitric oxide synthase: complementary roles of dual acylation and caveolin interactions. Biochemistry 37, 193–200.

Frank PG, Woodman SE, Park DS, Lisanti MP (2003). Caveolin, caveolae, and endothelial cell function. Artertioscler Thromb Vasc Biol 23, 1161–1168.

Furchgott RF, Zawadzki JV (1980). The obligatory role of endothelial cells in the relaxation of arterial smooth muscles by acetylcholine. Nature 288, 373–376.

García-Cardeña G, Fan R, Stern DF, Liu J, Sessa WC (1996). Endothelial nitric oxide is regulated by tyrosine phosphorylation and interacts with caveolin-1. J Biol Chem 271, 27237–27240.

García-Cardeña G, Martasek P, Masters BS, Skidd PM, Couet J, Li S, Lisanti MP, Sessa WC (1997). Dissecting the interaction between nitric oxide synthase (NOS) and caveolin. Functional significance of the nos caveolin binding domain in vivo. J Biol Chem 272, 25437–25440.

Ghosh S, Gachhui R, Crooks C, Wu C, Lisanti MP, Stuehr DJ (1998). Interaction between caveolin-1 and the reductase domain of endothelial nitric-oxide synthase. Consequences for catalysis. J Biol Chem 273, 22267–22271.

Grande-García A, Echarri A, de Rooij J, Alderson NB, Waterman-Storer CM, Valdivielso JM, del Pozo MA (2007). Caveolin-1 regulates cell polarization and directional migration through Src kinase and Rho GTPases. J Cell Biol 177, 683–694.

Gratton JP, Bernatchez P, Sessa WC (2004). Caveolae and caveolins in the cardiovascular system. Circ Res 94, 1408–1417.

Hu G, Schwartz DE, Shahajan AN, Visintine DJ, Salem MR, Crystal GJ, Albrecht RF, Vogel SM, Minshall RD (2006). Isoflurane, but not sevoflurane, increases transendothelial albumin permeability in the isolated rat lung: role for enhanced phosphorylation of caveolin-1. Anesthesiology 104, 777–785.

Hu G, Vogel SM, Visintine DJ, Schwartz DE, Malik AB, Minshall RD (2008). ICAM-1-dependent neutrophil adhesion to endothelial cells induces caveolae-mediated pulmonary vascular hyper-permeability. Circ Res 102, e120–e131.

Huang PL, Huang Z, Mashimo H, Bloch KD, Moskowitz MA, Bevan JA, Fishman MC (1995). Hypertension in mice lacking the gene for endothelial nitric oxide synthase. Nature 377, 239–242.

Jin ZG (2006). Where is endothelial nitric oxide synthase more critical: plasma membrane or Golgi? Arterioscler Thromb Vasc Biol 26, 959–961.

Joshi B *et al*. (2008). Rho/ROCK signaling acts via phospho-caveolin-1 to regulate focal adhesion dynamics and tumor cell migration. Cancer Res 68, 8210–8220.

Ju H, Zou R, Venema VJ, Venema RC (1997). Direct interaction of endothelial nitric-oxide synthase and caveolin-1 inhibits synthase activity. J Biol Chem 272, 18522–18525.

Kojima H, Nakatsubo N, Kikuchi K, Kawahara S, Kirino Y, Nagoshi H, Hirata Y, Nagano T (1998). Detection and imaging of nitric oxide with novel fluorescent indicators: diaminofluoresceins. Anal Chem 70, 2446–2453.

Maniatis NA, Shinin V, Schraufnagel DE, Okada S, Vogel SM, Malik AB, Minshall RD (2008). Increased pulmonary vascular resistance and defective pulmonary artery filling in caveolin-1-/- mice. Am J Physiol Lung Cell Mol Physiol 94, L865–L873.

Michel JB, Feron O, Sacks D, Michel T (1997a). Reciprocal regulation of endothelial nitric-oxide synthase by Ca2+-calmodulin and caveolin. J Biol Chem 272, 15583–15586.

Michel JB, Feron O, Sase K, Prabhakar P, Michel T (1997b). Caveolin versus calmodulin. Counterbalancing allosteric modulators of endothelial oxide synthase. J Biol Chem 272, 25907–25912.

Minshall RD, Tiruppathi C, Niles WD, Vogel SM, Gilchrist A, Hamm HE, Malik AB (2000). Endothelial cell surface gp60 activates vesicle formation and trafficking via G_i-coupled Src kinase signaling pathway. J Cell Biol 150, 1057–1069.

Monteiro HP, Gruia-Gray J, Peranovich TM, de Oliveira LC, Stern A (2000). Nitric oxide stimulates tyrosine phosphorylation of focal adhesion kinase, Src kinase, and mitogen-activated protein kinases in murine fibroblasts. Free Radic Biol Med 28, 174–182.

Nakatsubo N, Kojima H, Kikuchi K, Nagoshi H, Hirata Y, Maeda D, Imai Y, Irimura T, Nagano T (1998). Direct evidence of nitric oxide production from bovine aortic endothelial cells using new fluorescence indicators: diaminofluoresceins. FEBS Lett 427, 263–266.

Oess S, Icking A, Fulton D, Govers R, Müller-Esterl W (2006). Subcellular targeting and trafficking of nitric oxide synthases. Biochem J 396, 401–409.

Orlichenko L, Huang B, Krueger E, McNiven MA (2006). Epithelial growth factor-induced phosphorylation of caveolin 1 at tyrosine 14 stimulates caveolae formation in epithelial cells. J Biol Chem 281, 4570–4579.
Place AT, Chen Z, Bakhshi F, Liu G, O'Bryan JP, Minshall RD (2011). Cooperative role of caveolin-1 and Cbp in Csk-mediated negative regulation of c-Src. Mol Pharmacol 80, 665–672.
Radel C, Carlile-Klusacek M, Rizzo V (2007). Participation of caveolae in beta1 integrin-mediated mechanotransduction. Biochem Biophys Res Commun 358, 626–631.
Rahman MA, Senga T, Ito S, Hyodo T, Hasegawa H, Hamaguchi M (2010). S-Nitrosylation at cysteine 498 of c-Src tyrosine kinase regulates nitric oxide-mediated cell invasion. J Biol Chem 285, 3806–3814.
Raman CS, Li H, Martásek P, Král V, Masters BS, Poulos TL (1998). Crystal structure of constitutive endothelial nitric oxide synthase: a paradigm for pterin function involving a novel metal center. Cell 95, 939–950.
Razani B *et al*. (2001). Caveolin-1 null mice are viable but show evidence of hyperproliferative and vascular abnormalities. J Biol Chem 276, 38121–38138.
Sessa WC (2004). eNOS at a glance. J Cell Sci 117, 2427–2429.
Shajahan AN, Tiruppathi C, Smrcka AV, Malik AB, Minshall RD (2004). Gβγ activation of Src induces caveolae-mediated endocytosis in endothelial cells. J Biol Chem 279, 48055–48062.
Siddiqui MR, Komarova YA, Vogel SM, Gao X, Bonini MG, Rajasingh J, Zhao YY, Brovkovych V, Malik AB (2011). Caveolin-1-eNOS signaling promotes p190RhoGAP-A nitration and endothelial permeability. J Cell Biol 193, 841–850.
Smart EJ, Graf GA, McNiven MA, Sessa WC, Engelman JA, Scherer PE, Okamoto T, Lisanti MP (1999). Caveolins, liquid-ordered domains, and signal transduction. Mol Cell Biol 19, 7289–7304.
Sun Y, Hu G, Zhang X, Minshall RD (2009). Phosphorylation of caveolin-1 regulates oxidant-induced pulmonary vascular permeability via paracellular and transcellular pathways. Circ Res 105, 676–685.
Sverdlov M, Shajahan AN, Minshall RD (2007). Tyrosine phosphorylation-dependence of caveolae-mediated endocytosis. J Cell Mol Med 11, 1239–1250.
Sverdlov M, Shinin V, Castellon M, Place AT, Minshall RD (2009). Filamin A regulates caveolae internalization and trafficking in endothelial cells. Mol Biol Cell 20, 4531–4540.
Wang H, Wang AX, Liu Z, Chai W, Barrett EJ (2009). The trafficking/interaction of eNOS and caveolin-1 induced by insulin modulates endothelial nitric oxide production. Mol Endocrinol 23, 1613–1623.
Wang Y, Botvinick EL, Zhao Y, Berns MW, Usami S, Tsien RY, Chien S (2005). Visualizing the mechanical activation of Src. Nature 434, 1040–1045.
Wunderlich C, Schober K, Lange SA, Drab M, Braun-Dullaeus RC, Kasper M, Schwencke C, Schmeisser A, Strasser RH (2006). Disruption of caveolin-1 leads to enhanced nitrosative stress and severe systolic and diastolic heart failure. Biochem Biophys Res Commun 340, 702–708.
Zhao YY, Liu Y, Stan RV, Fan L, Gu Y, Dalton N, Chu PH, Peterson K, Ross J Jr, Chien KR (2002). Defects in caveolin-1 cause dilated cardiomyopathy and pulmonary hypertension in knockout mice. Proc Natl Acad Sci USA 99, 11375–11380.